

# Journal of Mechanics of Materials and Structures

**MECHANICAL BEHAVIOR  
OF SILICA NANOPARTICLE-IMPREGNATED  
KEVLAR FABRICS**

Zhaoxu Dong, James M. Manimala and C. T. Sun

**Volume 5, No. 4**

**April 2010**

 **mathematical sciences publishers**

## MECHANICAL BEHAVIOR OF SILICA NANOPARTICLE-IMPREGNATED KEVLAR FABRICS

ZHAOXU DONG, JAMES M. MANIMALA AND C. T. SUN

This study presents the development of a constitutive model for in-plane mechanical behavior of five styles of plain woven Kevlar fabrics impregnated with silica nanoparticles. The neat fabrics differed in fiber type, yarn count, denier, weave tightness and strength, and varying proportions (4, 8, 16 and 24% by weight) of nanoparticles were added to enhance the mechanical properties of the fabric. It was found that fabrics impregnated with nanoparticles exhibit significant improvement in shear stiffness and a slight increase in tensile stiffness along the yarn directions over their neat counterparts. A constitutive model was developed to characterize the nonlinear anisotropic properties of nanoparticle-impregnated fabrics undergoing large shear deformation. The parameters for the model were determined based on uniaxial (along yarn directions) and 45° off-axis tension tests. This model was incorporated in the commercial FEA software ABAQUS through a user-defined material subroutine to simulate various load cases.

### 1. Introduction

Kevlar<sup>®</sup> fiber is a high modulus, high strength and low density para-aramid synthetic fiber. In comparison to high strength steel, Kevlar has much better strength to weight ratio. It is a good candidate for use as a soft body protection material. The fibers are tightly woven into fabrics and multiple layers of fabrics are used in many soft body armors. The primary goal of soft armor design is to reduce the weight while maintaining the protection level. Hence, weight and performance are the two major criteria that must be balanced in selecting soft body armors.

The mechanical behavior of Kevlar fabrics under uniaxial tensile loading has been extensively studied previously. Raftenberg and Mulkern [2002] performed uniaxial tension tests on Kevlar KM2 yarn and fabric to obtain stress versus displacement curves. They also obtained bilinear, exponential and quartic least square error fits to the data. The shear response of E-glass fabrics of various weave styles was studied in [Mohammed et al. 2000] using picture frame tests. The locking angle was determined for each type of weave. A material model based on the theory of elasticity including the effect of fiber inextensibility was applied to analyze the experimental data and a microstructural analysis was done to predict the shear locking angle. Peng et al. [2004] address the issue of comparing fabric shear test data obtained from different testing methods. It was found that the normalization method to be employed depended on the experimental configuration of the test. Lomov et al. [2006] investigated the factors affecting the validity of data obtained from picture frame tests on glass/PP woven fabrics. They also report that yarn pretension caused difference in the shear resistance measured for the fabric. Controlling the pretension

---

*Keywords:* Kevlar fabric, soft armor, nanoparticle, constitutive model.

in the yarn during sample preparation and standardizing testing procedures were recommended to obtain more accurate shear response using the picture frame test. Further, we cite [Harrison et al. 2004; Lebrun et al. 2003; Milani et al. 2010] as comparative studies on the evaluation of the in-plane shear behavior of fabrics using the bias extension and the picture frame tests.

Researchers have been continuously looking for ways to lighten body armors without compromising on performance. One way is to create stronger and lighter fibers by producing new materials and processes. Another method is to tailor the structure and composition of existing fabrics to achieve better performance. Lee et al. [2003] reported a significant enhancement in ballistic performance of Kevlar woven fabrics when impregnated with a shear thickening fluid (STF). The STF used was a colloid of ethylene glycol and highly concentrated silica nanoparticles. The viscosity of the STF increases significantly above a critical shear rate. This novel STF-fabric material offers good ballistic resistance and flexibility. However, the enhancement mechanisms and the exact role of STF in strengthening the fabric are still not well understood. In [Decker et al. 2007; Kalman et al. 2009] it was demonstrated that STF Kevlar fabrics offered better stab resistance properties than neat Kevlar by restricting the yarn mobility. Tan et al. [2005] impregnated Twaron<sup>®</sup> fabrics with a water based silica colloid. Improvement in ballistic resistance was observed, and they attributed it to the increase in projectile-fabric and inter-yarn friction.

Many different approaches like simplified orthogonal pin-jointed bars to model yarns, unit cell based models, equivalent homogenized continuum models and detailed three-dimensional models incorporating individual yarns and weave patterns with contact definitions have been used to analyze and model woven fabric material behavior. King et al. [2005] developed a continuum constitutive model for woven fabrics in which the fabric yarn structural configuration is related to the macroscopic deformation through an energy minimization method. Lin et al. [2009] developed a finite element model to predict the shear force versus shear angle response of a plain woven fabric. The fabric was modeled at the yarn scale by assuming yarn behavior to be that of a three-dimensional orthotropic solid. In [Grujicic et al. 2009], a meso-scale (yarn level) unit cell was developed and its properties were used to model plain woven Kevlar 129 fabric as a continuum surface via a user-defined material subroutine in ABAQUS. The properties of the unit cell were obtained from contact forces and shear response of a solid FEM model of cross yarns in a single unit cell.

In the present study, dry silica nanoparticles were used to reinforce Kevlar fabrics. Unlike the STF-fabric material, these nanoparticle-fabric composites do not contain any fluid and thus minimizes the weight added to neat fabrics. Uniaxial and 45° off-axis tension tests were done to evaluate the in-plane mechanical properties of the fabrics using an MTS servo-hydraulic load frame. It was found that the nanoparticles significantly increased the in-plane shear stiffness, while only slightly influenced the tension behavior along yarn directions. All the tested fabrics exhibited highly nonlinear behavior in shear deformation and large relative rotations between cross yarns. A constitutive model was developed using a method similar to the classical laminated plate theory in conjunction with the incremental deformation approach to characterize the nonlinear anisotropic properties of nanoparticle-impregnated fabrics undergoing large deformation. This model was incorporated in the commercial FEA software ABAQUS via a user-defined material (UMAT) subroutine to simulate the mechanical response of Kevlar fabrics. Validation of the model was done by comparing the numerical results to experimental load displacement curves for a 30° off-axis tension test and static indentation tests. The simulations agree well with the experimental results until the onset of failure.

Fabric style	K310	K706	K720	K745	K779
Fiber type	Comfort	KM-2	129	29	159
Fiber modulus (GPa)	87.0	80.0	99.7	73.0	97.2
Yarn size (denier)	400	600	1420	3000	200
Weight (g/m <sup>2</sup> )	122	180	258	475	132
Warp count (yarns/in)	35.5	34	20	17	70
Weft count (yarns/in)	35.5	34	20	17	70
Warp strength (lbs/in)	530	775	978	1600	385
Weft strength (lbs/in)	530	880	992	1800	530
Thickness (mm)	0.18	0.23	0.36	0.61	0.18

**Table 1.** Manufacturer's product data of five styles of plain woven Kevlar fabrics.

## 2. Experimental methods

**2.1. Material preparation.** Five styles of Kevlar fabrics from Hexcel<sup>®</sup> were studied. The fabric specifications given by the manufacturer are listed in Table 1. These fabrics differ in fiber type, yarn size, yarn count, weave tightness, thickness, strength and weight. All the styles were, however, plain woven fabrics. Figure 1 shows the weave texture of these fabrics. K779 style has a fine, tight weave; K310 and K706 have medium weaves; K720 and K745 are thick and heavy styles with coarse and loose yarns. The fabric properties are sensitive to ultraviolet radiation and moisture absorption. Hence the fabric rolls were stored in a closed dry container and the samples were oven dried to remove ambient moisture prior to testing.

Plain woven fabrics have two orthogonal yarn directions — warp and weft — in the undeformed configuration (Figure 2a). Although the fabric is balanced and has the same yarn count in the warp and weft directions, their strengths are different. It is therefore necessary to identify them. If the selvage is still on the fabric, the yarns that are parallel to the selvage are the warp yarns. Alternatively, the warp and weft yarns can be distinguished by their waviness. Due to the weaving process, the warp yarns have more waviness than the weft yarn. Figure 2b shows an extracted warp and weft yarn from K720 style fabric.

A water-based silica nanoparticle colloid (Snowtex<sup>®</sup> ST-ZL) marketed by Nissan Chemical was used to impregnate nanoparticles into the fabric. According to the manufacturer's specifications, the silica

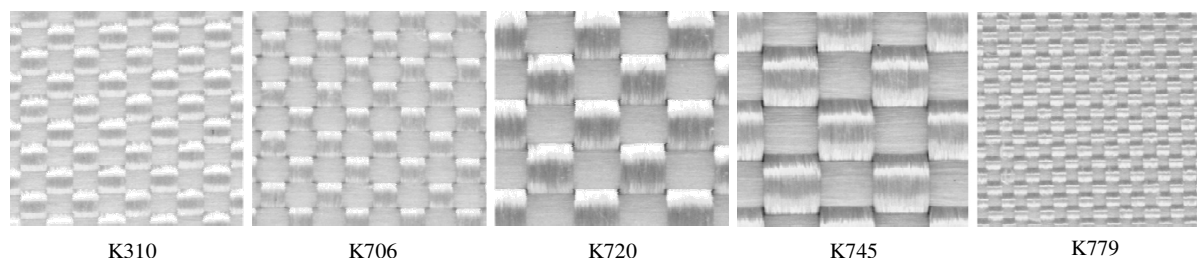


**Figure 1.** Optical images of five styles of plain woven Kevlar fabrics. (Each image corresponds to  $6.4 \times 6.4$  mm. The fabrics are bright yellow; the images were postprocessed to black and white to enhance the contrast.)

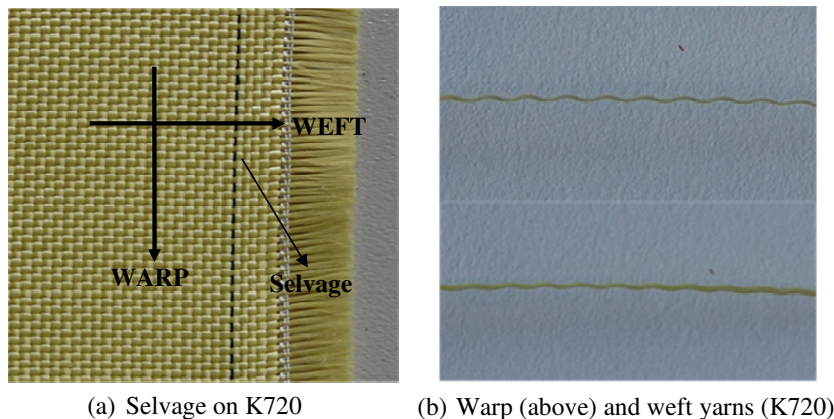


**Figure 2.** Identifying warp and weft yarns in the fabric: warp yarns are wavier than weft yarns.

particle size was 70~100 nm and the particle concentration was 40~41% by weight. To impregnate the silica nanoparticles into the fabric, a square piece of fabric of dimensions  $150 \times 150$  mm was cut from the bulk fabric roll. The weight of the fabric was measured and recorded using an OHAUS<sup>®</sup> analytical balance. It was then soaked into the silica colloid and the percentage by weight of the solution added to the fabric was controlled. The soaked piece was oven dried at 80° C for 30 minutes to remove the water leaving silica nanoparticles adhered to the fabric. The final nanoparticle weight additions to the neat fabrics are controlled to be 4, 8, 16 and 24%. The resulting nanoparticle impregnated fabric remained quite flexible albeit not as much as the neat fabric. Figure 3 shows the scanning electron micrograph (SEM) of K706 with 24 wt% of silica nanoparticles. Samples were imaged with an FEI Nova NanoSEM field emission scanning electron microscope. The image was obtained using back-scatter detector in low vacuum mode. The image reveals that silica nanoparticles did not form a uniform coating on the fabric surface but accumulated in the space between fibers. Abrading the surface of the treated fabric dislodges only the particles adhering to the surface but the particles in the interfiber spaces remain undisturbed.

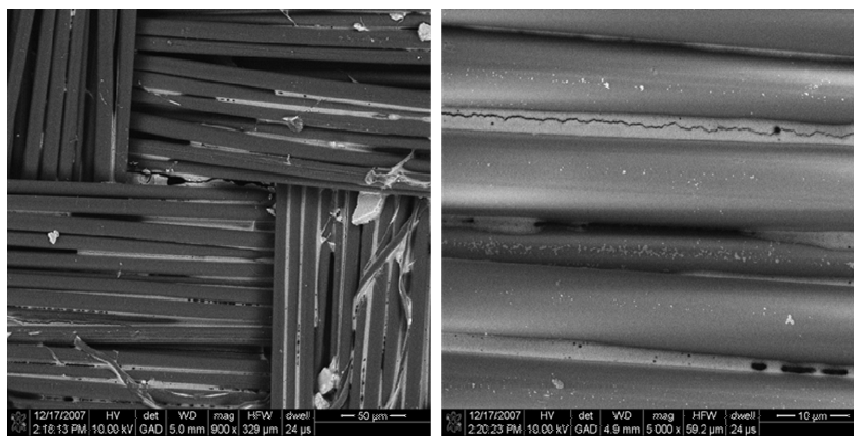


**Figure 3.** SEM image of K706 fabric with 24 wt% silica nanoparticles.

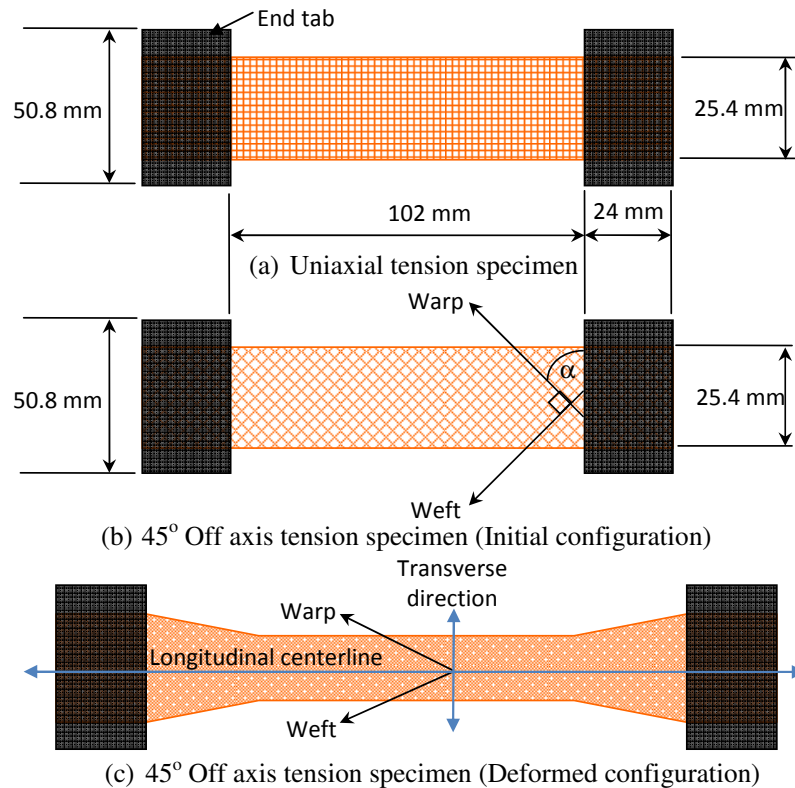


**Figure 4.** Diagram of tension test specimen.

**2.2. Uniaxial tension tests.** To evaluate the yarn direction stiffness of the fabrics, quasistatic uniaxial tension tests were performed on the neat and nanoparticle impregnated fabrics. The fabrics (single layer) with different wt% additions of nanoparticles were tested in both the warp and the weft directions. To prepare the specimens for the test, the neat and treated fabrics were cut into a rectangular piece of 25.4 mm in width and 150 mm in length along the yarn directions. Hard end tabs were bonded using epoxy adhesive to both ends leaving a gauge length of 102 mm between the tabs. Figure 4a shows the dimensions of the final specimen. A 100 kN MTS load frame was used in this test. The crosshead speed was set to 0.1 mm/second. The specimen was aligned and gripped using hydraulic grips during the test. No slippage at the grips was noticed during testing.

**2.3. Off-axis tension tests.** Picture frame tests are widely used to evaluate the in-plane shear properties of woven fabrics [Mohammed et al. 2000; Peng et al. 2004; Lomov et al. 2006]. The stress field in the picture frame is usually assumed to be uniform. When shear deformation is small, the fabric does not wrinkle and the uniform stress assumption is reasonable. However, the fabric wrinkles under large shear deformations. This results in nonuniform stress distributions and the accuracy of the test result is not guaranteed.

In view of the foregoing, we employed a 45° off-axis tension (bias extension) test to determine the fabric shear property. The specimen size was the same as that used in the uniaxial tension tests. Parts b and c of Figure 4 show the initial and deformed configurations. The yarn orientation angle  $\alpha$  is the

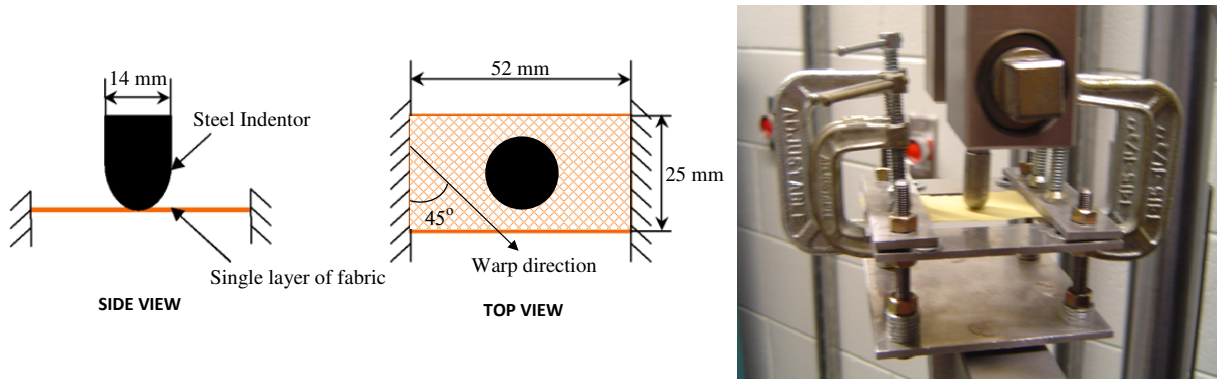


**Figure 5.** Left: schematic diagram of static indentation test. Right: indentation test on neat K706.

acute angle made by the warp direction yarn with the short (25 mm) edge of the specimen, as shown in Figure 4b. The specimens were cut in such a way that this angle was  $45^\circ$  in the undeformed state. As the warp and weft directions in the fabric are orthogonal to each other initially, this test has a symmetric configuration with respect to both yarn directions. The specimens were tabbed and tested with same experimental setup as the uniaxial tension tests. No slippage at the grips was noticed during testing.

The uniaxial and the  $45^\circ$  off-axis tension tests are used to obtain the material parameters for the constitutive model. In order to validate the model, one of the load cases used was a  $30^\circ$  off-axis tension test. The test was done using K706 fabric style with the same specimen dimensions and test conditions as for the  $45^\circ$  off-axis tension tests.

**2.4. Indentation test.** Under a transverse ballistic impact, the major mode of deformation in Kevlar fabrics is the out-of-plane displacement. Static indentation tests display certain correlations especially with regard to deformed profile, yarn pull-out behavior and indenter-yarn diameter size effects to the behavior of the fabric during ballistic impact. However, in ballistic tests, dynamic phenomena such as strain rate dependence and wave propagation effects become evident. To evaluate the accuracy of the proposed constitutive model, a static indentation test was done. The indentation test setup and specimen dimensions are schematically shown in Figure 5, left. A single layer of K706 Kevlar fabric with a yarn orientation angle of  $45^\circ$  was wrapped and clamped without slack between the grips of the test fixture such that two opposite edges are fixed and the other two edges are free. A hemispherical indenter of diameter 14 mm was pushed against the fabric at a crosshead speed of 0.1 mm/second using an MTS load frame and the load versus displacement response was recorded. No slippage at the gripped edges was noticed until onset of failure. Figure 5, right, shows an indentation test in progress.

### 3. Experimental results

**3.1. Uniaxial tension tests.** The uniaxial tension tests for the fabrics show two distinct regimes in the load displacement plots. In the initial loading phase the fabric has a linear behavior with low modulus. The axial strain occurs during this phase primarily because of the uncrimping of the axial yarns in the woven fabric. In the absence of any applied transverse tension, the actual phenomenon is one of crimp interchange whereby the axial yarns get straightened while the transverse yarns take up additional crimp.

However, once the axial yarns become uncrimped, the transverse yarns remain in position and no pullout is noticed. In the later loading phase the axial yarns undergo elongation with a relatively higher modulus. The yarn elongation response is also linear until the fabric fails by the breakage of axial yarns. The failure location depends on the location of any local defects but occurs at a definite load and is obtained consistently in repeated tests. The uniaxial response is thus markedly bilinear. The results show that, in general, the weft yarns are stronger than the warp yarns and also display a stiffer response. The addition of nanoparticles to the fabrics seems to increase the uniaxial strength and stiffness only slightly as evidenced by the plots presented in Figure 6. Nonetheless, we make a few observations of interest.

Firstly, as the deformation progresses, it is noticed that the width of the specimen remains more or less unchanged. Unlike a homogenous solid, the deformation in fabrics is largely governed by interaction between yarns at the cross over points in the weave. But once the crimp interchange process is complete after the initial loading phase, no transverse yarn pull out is noticed, which indicates that the width of the specimen (distance between outer most axial yarns) remains the same as the initial width of the specimen. This was noted to be the case for all the specimens tested and thus an assumption of negligible lateral contraction is made for the fabric loaded in uniaxial tension.

As the crimp interchange process reduces the yarn waviness in the axial direction while increasing it in the transverse direction, the variation of the overall thickness of the fabric is very small. Variability in the load sensed by individual axial yarns is reduced by ensuring high precision in the specimen fabrication process and alignment and gripping procedure for the test. However one of the factors affecting the scatter in the failure location (apart from any local defects) may be the slight difference in pretension induced due to errors in the aforesaid procedures. Owing to the existence of these conditions in the fabric during the uniaxial tension test, it is reasonable to assume a state of uniform axial stress and strain field. Hence, engineering stress versus strain can be reported using the initial specimen dimensions, which are presented in Figure 6. The thickness of woven fabrics is measured using ASTM D1777-96 standard. The thickness values as quoted by the manufacturer (Table 1) are used to calculate the fabric cross sectional area. The warp and weft fabric strengths as obtained from the tests (Table 2) differ from the manufacturer supplied values given in Table 1. The average difference between measured and supplied value is about 16%. As the manufacturer's test procedure is not supplied with the material data sheet, the variation in the measured strength values is attributed to difference in test methods and conditions. The axial mechanical properties of the fabric are obtained from the test results using a bilinear curve fit. The strength values assume significance only in the context of failure prediction which is not dealt with in the present study.

Secondly, a comparison of the load displacement curves for various styles of fabrics shows a slight departure from the typical trend for certain styles. In general it is noted that the weft direction has lower strains to complete uncrimping, higher moduli in both load regimes and greater strength. This is explained by the fact that the weft yarns are much less wavy than warp yarns and as a consequence

Fabric style	K310	K706	K720	K745	K779
Weight (g/m <sup>2</sup> )	127	178	254	435	127
Warp strength (lbs/in)	630	760	1220	1770	390
Weft strength (lbs/in)	730	970	1290	1910	670

**Table 2.** Neat fabric weights and strengths measured in this study.

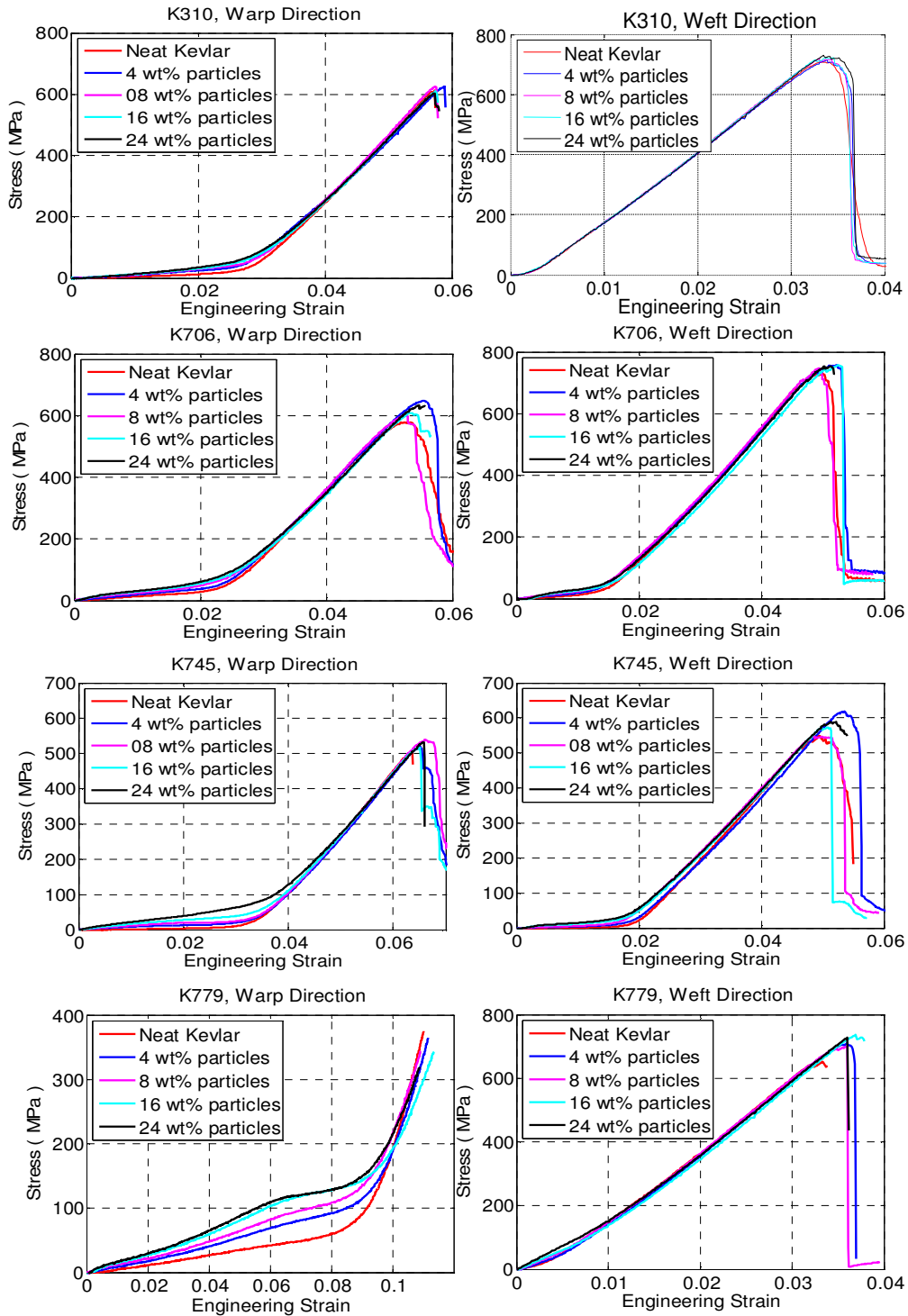


**Figure 6.** Engineering stress versus strain curves from uniaxial tension tests for five styles of Kevlar fabrics with different wt% of nanoparticle addition.

are fully uncrimped at lower strain values. The bilinear transition strain for most neat and treated fabric styles is between 0.01 and 0.03. However, K310 and K779 styles are exceptions. Among the five styles of fabric tested, K779 and K310 have the finest and the second finest weave respectively. Both these fabrics are tightly woven with very close yarn spacing. The steep rise in the weft direction load displacement curves for K310 and K779 is due to their fine weave which causes the yarn to become fully uncrimped at very low strains. This is less evident in the warp direction because of its relatively higher waviness.

The mechanism by which the addition of nanoparticles increases the stiffness of the fabric is conjectured to be due to increase in the friction between the yarns. As the nanoparticles are embedded in the interyarn and interfiber spaces, they restrict the relative yarn mobility. This effect becomes more pronounced in the case of fine weave fabrics in comparison to coarse weave as the nanoparticles are lodged in very small gaps between the tightly woven yarns. In the case of the warp direction response for K779, because of the high waviness and fine weave, the initial resistance to applied strain is due to a combination of elongation of the yarns and uncrimping as the nanoparticles lock the yarns in place relative to each other. Once the frictional resistance due to the nanoparticles is overcome a short plateau phase is observed when the uncrimping process is completed and thereafter the yarns undergo axial elongation alone until failure. This could be the reason for the high dependence of the initial load displacement response of weft direction K779 fabric on the percentage weight addition of nanoparticles.

**3.2. Off-axis tension tests.** The mechanical behavior exhibited by neat and treated fabrics in a 45° off-axis tension test offer numerous insights. The load displacement curves are highly nonlinear and the addition of nanoparticles to the fabric causes a significant increase in its shear rigidity and failure strength. Figure 7 presents the load versus displacement plots for five styles of Kevlar fabrics with different wt% additions of nanoparticles.

In an off-axis tension test, the deformation of the fabric is dependent on the specimen dimensions, yarn orientation angle, yarn count in warp and weft directions and the nanoparticle loading of the fabric. For balanced plain woven Kevlar fabrics with the same yarn count in warp and weft directions, a 45° off-axis tension (bias extension) test produces a deformation that is symmetric about the longitudinal center line of the specimen (Figure 4c). Distinct shear regions are observed in the specimen during deformation [Harrison et al. 2004; Lebrun et al. 2003]. The central region *C*, as shown in Figure 8 (page 539) has a pure shear deformation as the yarns experience only rotations relative to each other, while the region *A* remains undeformed and region *B* has a shear angle half that in region *C*. Due to the rotation of the yarns, region *C* displays large transverse contraction. The length of region *C* depends on the specimen dimensions and yarn count of the fabric. The load displacement curves show a steep rise after a critical value of displacement is reached in each case. This occurs because as the yarn rotations progress, a limiting angle is reached when adjacent yarns become compactly packed without any interyarn spacing. This angle is referred to as the locking angle for fabrics. After the locking angle is reached the shear rigidity of the fabric is driven by the compression of individual yarns in the transverse direction which causes a greater load to be sensed per unit displacement. In the postlocking deformation, out-of-plane wrinkling of the fabrics occur. Failure initiation occurs thereafter by the slipping of the yarns at the interface between shear regions *C* and *B*. Unlike the uniaxial tension test, the failure does not occur at a well defined load but progresses gradually as weft and warp yarns slip over each other at cross over points. The oscillatory behavior in the curves at displacements close to failure is due to this phenomenon

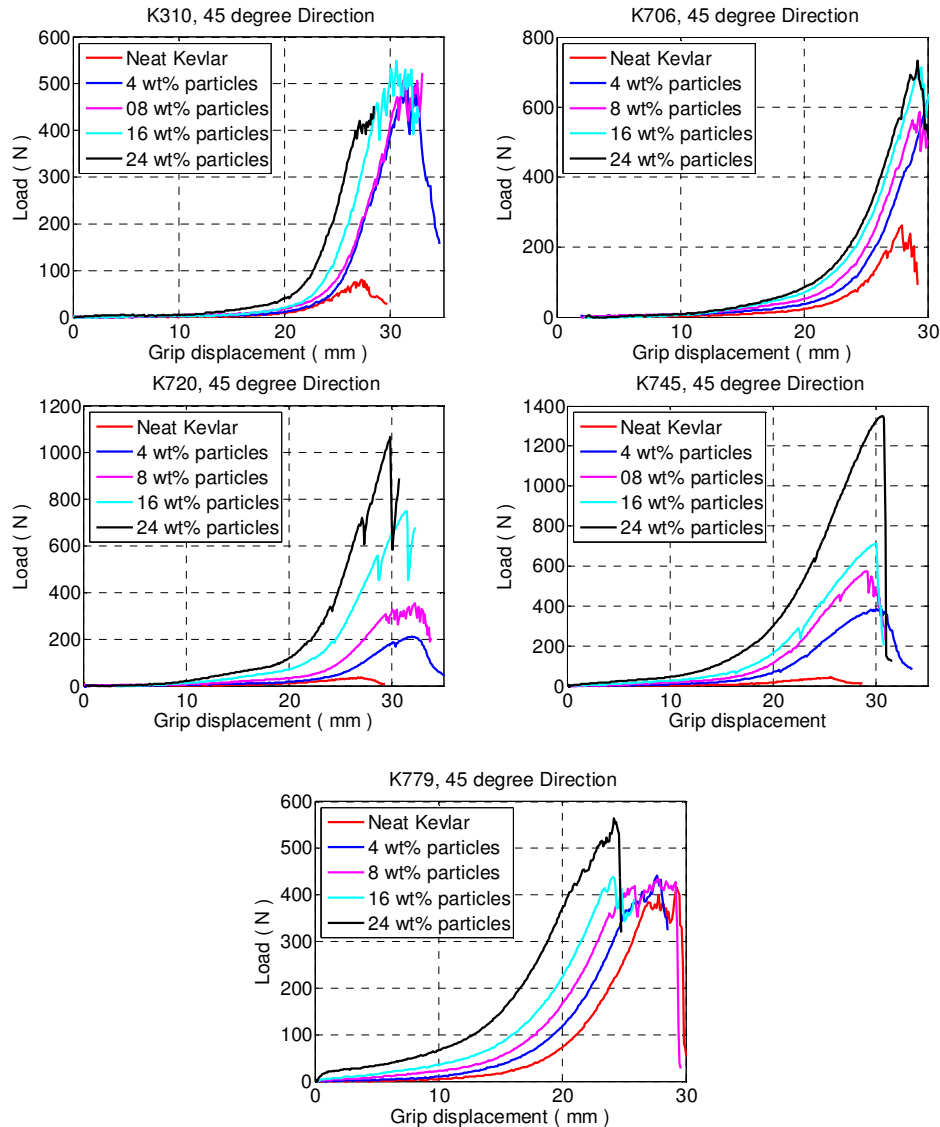


**Figure 7.** Load versus displacement curves from 45° off-axis tension tests for five styles of Kevlar fabrics with different wt% addition of nanoparticles.

of yarn sliding at corners. The maximum load is sensed during the yarn sliding phase after which the curve falls rapidly as the two portions of the specimen separate. The failure location was always observed to be at either the upper or lower shear region interfaces. The addition of nanoparticles did not affect the location of failure. However, treated fabrics display a more definite failure load as the enhanced load carrying ability diminishes rapidly once the nanoparticles that lock the relative motion between adjacent yarns are dislodged. This reinforces the inference that the nanoparticles enhance the shear rigidity by increasing the interyarn and intrayarn friction in woven fabrics.

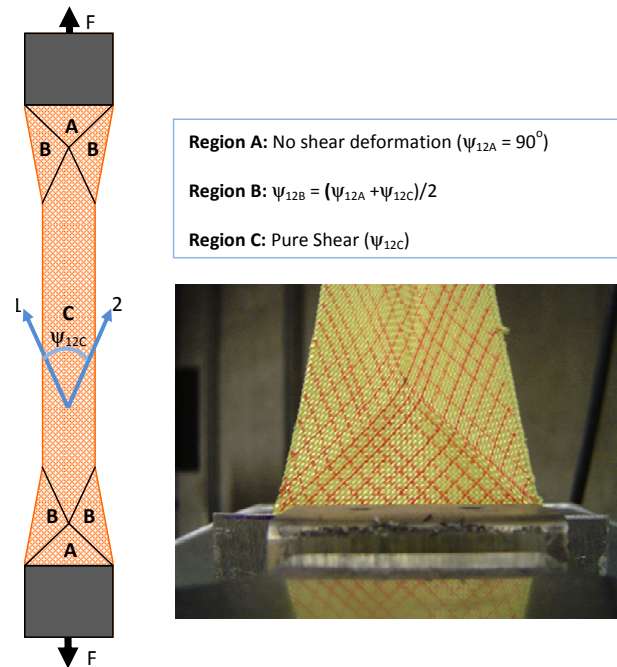


**Figure 8.** Shear regions in a 45° off-axis tension test: schematic diagram and actual deformation.

The load displacement plots (Figure 7) demonstrate that substantial enhancement of shear rigidity and strength is achieved by the addition of nanoparticles to the fabric. The effect is greater for coarse weave fabrics which have low rigidity in the neat condition. K745 (the coarsest weave among the five styles) registers a failure load of nearly 26 times that of its neat strength with an addition of 24% by weight of nanoparticles. In comparison, fine weave fabrics that have higher interyarn friction in the neat state due to their smaller yarn size and interyarn spacing, show lower sensitivity to the percentage of nanoparticles added. K779, for example, shows a proportional increase in stiffness with increase in the amount of nanoparticles added but the failure load remains more or less the same. It is surmised that the impregnation of nanoparticles in the fabric imparts an additional mechanism of frictional interaction between the yarns which acts in conjunction with the inherent interyarn friction present in neat fabrics. In the case of fine weave fabrics like K779, the effect of the neat fabric friction is predominant and hence the fabric shows lower increase in failure load with increase in nanoparticle addition. The fabric styles K310, K706 and K720 show varying degrees of increase in shear rigidity and failure loads. An important factor that influences the behavior of silica nanoparticle impregnated fabrics is the uniformity of the distribution of nanoparticles in the fabric. Although, the process is controlled to ensure that the nanoparticle colloid soaks the fabric evenly and remains undisturbed during the drying process, SEM images reveal that there is agglomeration of particles in interyarn spaces. Hence, to a certain extent, variability in the failure load of the fabric may be attributed to the nonuniform distribution of nanoparticles in the fabric.

**3.3. Indentation test.** Indentation test was conducted for validation of the constitutive model. The deformation and failure of Kevlar fabrics in a static indentation test depends on the fabric style, indenter size

and boundary conditions. As a  $45^\circ$  yarn orientation was used, large out-of-plane deformation occurs before failure initiation. Unlike the off-axis tension test, the yarn rotations in the specimen are not uniform. The indenter load is initially small as the out-of-plane deformation is accommodated by uncrimping of yarns. Once the rotations of the yarns are close to the locking value, a steep rise in the indenter load is noticed. Further transverse displacement leads to the onset of failure by the sliding (unraveling) of yarns at cross over points at the corner of the clamped edges of the specimen.

#### 4. Constitutive modeling

The uniaxial and off-axis tension tests reveal that Kevlar fabrics have very high stiffness in both yarn directions, but a very low in-plane shear resistance. Addition of nanoparticles produces a substantial increase in shear rigidity while only a small increase is obtained in the axial stiffness. The tensile strains in yarn directions are small because of high stiffness in these directions. However, an in-plane shear loading can cause very large changes in the angle between the warp and weft yarns due to their relative rotations. This behavior makes the modeling of the fabric as a homogenized continuum rather difficult. In addition, for nanoparticle impregnated fabrics, the effect of the nanoparticles on the mechanical behavior must be included in the constitutive equations.

To simplify this task, we adopt an incremental deformation approach in setting up the constitutive model in conjunction with a procedure that resembles the classical laminated plate theory. As the response of the fabrics is highly nonlinear, an incremental deformation approach is used. At every increment, the fabric deforms through the interaction of the warp and weft families of yarns. This interaction is simplified by modeling the warp and weft yarns as two separate plies in a composite laminate. Once the incremental constitutive equations are established, they can be implemented as a user defined subroutine in the commercial finite element code ABAQUS/ Standard to perform numerical simulations.

A set of coordinate systems are established as shown in Figure 9. The fabric is assumed to lie in the  $x$ - $y$  plane with the warp and weft yarns initially assumed to be oriented at angles  $\alpha$  and  $\beta$  respectively to the positive  $x$  direction of the global coordinate system  $x$ - $y$ . An angle measured anticlockwise from the positive  $x$  direction is represented as positive and an angle measured clockwise is represented as negative. As the out-of-plane thickness of the fabric is very small compared to the specimen in-plane dimensions, an assumption of a state of plane stress is made. For plain woven fabrics the warp and weft directions are orthogonal to each other in the undeformed condition. As the fabric undergoes large shear deformations, the yarns rotate relative to each other and the angle between them in the deformed state

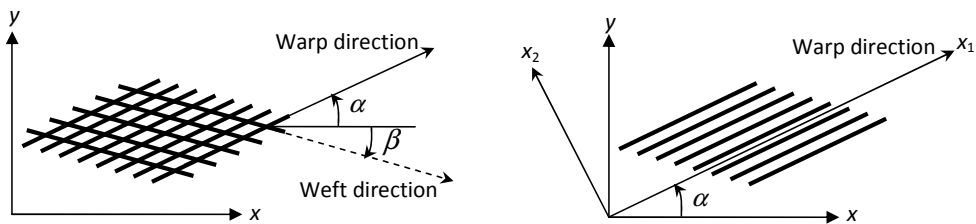


**Figure 9.** Left: global coordinate system  $(x, y)$  and yarn orientations. Right: Local coordinate system  $(x_1, x_2)$  for the warp layer.

( $\theta$ ) can become much larger or smaller than  $90^\circ$ . Two local coordinate systems,  $(x_1, x_2)_\alpha$  and  $(x_1, x_2)_\beta$  are established for the warp and the weft layers respectively such that the  $x_1$  direction is along the yarn direction in each layer.

At each incremental step, a single layer of Kevlar fabric of thickness  $T$  is modeled as the composite of two layers of unidirectional fibers. The effective mechanical properties of each layer are modeled as a two-dimensional orthotropic solid and the fabric is modeled as the laminate consisting of two fiber layers. Considering the warp layer, the incremental stress-strain relations for this layer are formulated in the local coordinate system as

$$\begin{Bmatrix} \Delta\sigma_{11} \\ \Delta\sigma_{22} \\ \Delta\sigma_{12} \end{Bmatrix} = \begin{bmatrix} \frac{E_1^\alpha}{1-\nu_{12}\nu_{21}} & \frac{\nu_{12}^\alpha E_2^\alpha}{1-\nu_{12}^\alpha\nu_{21}^\alpha} & 0 \\ \frac{\nu_{12}^\alpha E_2^\alpha}{1-\nu_{12}^\alpha\nu_{21}^\alpha} & \frac{E_2^\alpha}{1-\nu_{12}^\alpha\nu_{21}^\alpha} & 0 \\ 0 & 0 & G_{12}^\alpha \end{bmatrix} \begin{Bmatrix} \Delta\varepsilon_{11} \\ \Delta\varepsilon_{22} \\ \Delta\gamma_{12} \end{Bmatrix}, \quad (1)$$

where the superscript  $\alpha$  denotes the warp layer and  $E_1^\alpha$ ,  $E_2^\alpha$  and  $\nu_{12}^\alpha$  are the yarn direction modulus, transverse modulus and in-plane Poisson's ratio for the layer. The uniaxial tension tests show that for an applied tensile load in the yarn directions, the fabric structure does not have any overall contraction in the transverse direction. The yarns themselves (which are formed by bundles of fibers) may contract leading to an increase in the free space between yarns, but the overall transverse dimension of the specimen remains unchanged. Thus from a continuum perspective, the in-plane Poisson's ratio for a layer of unidirectional yarns (warp or weft) is negligible and is set to zero which simplifies Equation (1) to

$$\begin{Bmatrix} \Delta\sigma_{11} \\ \Delta\sigma_{22} \\ \Delta\sigma_{12} \end{Bmatrix} = \begin{bmatrix} E_1^\alpha & 0 & 0 \\ 0 & E_2^\alpha & 0 \\ 0 & 0 & G_{12}^\alpha \end{bmatrix} \begin{Bmatrix} \Delta\varepsilon_{11} \\ \Delta\varepsilon_{22} \\ \Delta\gamma_{12} \end{Bmatrix}. \quad (2)$$

The incremental stress-strain relations for the warp layer in the global coordinate system  $x$ - $y$  can now be obtained using coordinate transformation as

$$\begin{Bmatrix} \Delta\sigma_{xx} \\ \Delta\sigma_{yy} \\ \Delta\sigma_{xy} \end{Bmatrix} = \begin{bmatrix} Q_{11}^\alpha & Q_{12}^\alpha & Q_{16}^\alpha \\ Q_{12}^\alpha & Q_{22}^\alpha & Q_{26}^\alpha \\ Q_{16}^\alpha & Q_{26}^\alpha & Q_{66}^\alpha \end{bmatrix} \begin{Bmatrix} \Delta\varepsilon_{xx} \\ \Delta\varepsilon_{yy} \\ \Delta\gamma_{xy} \end{Bmatrix} = [Q^\alpha] \begin{Bmatrix} \Delta\varepsilon_{xx} \\ \Delta\varepsilon_{yy} \\ \Delta\gamma_{xy} \end{Bmatrix}, \quad (3)$$

where the reduced stiffnesses for the warp layer,  $Q_{ij}^\alpha$ , are given by

$$\begin{aligned} Q_{11}^\alpha &= E_1^\alpha \cos^4 \alpha + 4G_{12}^\alpha \sin^2 \alpha \cos^2 \alpha + E_2^\alpha \sin^4 \alpha, \\ Q_{12}^\alpha &= (E_1^\alpha + E_2^\alpha - 4G_{12}^\alpha) \sin^2 \alpha \cos^2 \alpha, \\ Q_{22}^\alpha &= E_1^\alpha \sin^4 \alpha + 4G_{12}^\alpha \sin^2 \alpha \cos^2 \alpha + E_2^\alpha \cos^4 \alpha, \\ Q_{16}^\alpha &= (E_1^\alpha - 2G_{12}^\alpha) \sin \alpha \cos^3 \alpha - (E_2^\alpha - 2G_{12}^\alpha) \sin^3 \alpha \cos \alpha, \\ Q_{26}^\alpha &= (E_1^\alpha - 2G_{12}^\alpha) \sin^3 \alpha \cos \alpha - (E_2^\alpha - 2G_{12}^\alpha) \sin \alpha \cos^3 \alpha, \\ Q_{66}^\alpha &= (E_1^\alpha + E_2^\alpha - 2G_{12}^\alpha) \sin^2 \alpha \cos^2 \alpha + G_{12}^\alpha (\sin^4 \alpha + \cos^4 \alpha). \end{aligned} \quad (4)$$

Similarly the incremental stress-strain relations in the global coordinate system for the weft layer are obtained as

$$\begin{Bmatrix} \Delta\sigma_{xx} \\ \Delta\sigma_{yy} \\ \Delta\sigma_{xy} \end{Bmatrix} = \begin{bmatrix} Q_{11}^\beta & Q_{12}^\beta & Q_{16}^\beta \\ Q_{12}^\beta & Q_{22}^\beta & Q_{26}^\beta \\ Q_{16}^\beta & Q_{26}^\beta & Q_{66}^\beta \end{bmatrix} \begin{Bmatrix} \Delta\varepsilon_{xx} \\ \Delta\varepsilon_{yy} \\ \Delta\gamma_{xy} \end{Bmatrix} = [Q^\beta] \begin{Bmatrix} \Delta\varepsilon_{xx} \\ \Delta\varepsilon_{yy} \\ \Delta\gamma_{xy} \end{Bmatrix}. \quad (5)$$

The superscript  $\beta$  denotes the weft layer and the reduced stiffnesses for the weft layer,  $Q_{ij}^\beta$ , are given by

$$\begin{aligned} Q_{11}^\beta &= E_1^\beta \cos^4 \beta + 4G_{12}^\beta \sin^2 \beta \cos^2 \beta + E_2^\beta \sin^4 \beta, \\ Q_{12}^\beta &= (E_1^\beta + E_2^\beta - 4G_{12}^\beta) \sin^2 \beta \cos^2 \beta, \\ Q_{22}^\beta &= E_1^\beta \sin^4 \beta + 4G_{12}^\beta \sin^2 \beta \cos^2 \beta + E_2^\beta \cos^4 \beta, \\ Q_{16}^\beta &= (E_1^\beta - 2G_{12}^\beta) \sin \beta \cos^3 \beta - (E_2^\beta - 2G_{12}^\beta) \sin^3 \beta \cos \beta, \\ Q_{26}^\beta &= (E_1^\beta - 2G_{12}^\beta) \sin^3 \beta \cos \beta - (E_2^\beta - 2G_{12}^\beta) \sin \beta \cos^3 \beta, \\ Q_{66}^\beta &= (E_1^\beta + E_2^\beta - 2G_{12}^\beta) \sin^2 \beta \cos^2 \beta + G_{12}^\beta (\sin^4 \beta + \cos^4 \beta). \end{aligned} \quad (6)$$

The warp and weft layers exist in an interwoven state in the actual fabric and hence to simplify the formulation, we assume that both layers occupy the same space and have the same thickness ( $T$ ) which is the thickness of one fabric layer. This thickness is set to be constant over the fabric undergoing large deformation. To be consistent, material properties for the warp and weft layers are defined using the thickness. Thus, the stiffness matrix for the fabric is obtained as

$$[Q] = [Q^\alpha] + [Q^\beta]. \quad (7)$$

Equation (7) provides the stiffness matrix for a single layer of fabric which is dependent on a total of six unknown material parameters – three each for warp and weft yarn directions. For each layer, the moduli  $E_1$ ,  $E_2$  and  $G_{12}$  are calibrated from the uniaxial and off-axis tension tests. These moduli must reflect the variation in yarn spacing under large deformations due to relative rotation of warp and weft yarns. True strain and true stress are used in the ABAQUS incremental formulation. In the following discussion, neat Kevlar K706 style fabric will be used as an example to illustrate the procedure for obtaining the material parameters. The same procedure is followed for other styles of neat and treated fabrics.

The uniaxial tension tests in the warp and weft directions display a bilinear trend. Hence, a simple bilinear function was used to approximate the tangent longitudinal moduli  $E_1^\alpha$  and  $E_1^\beta$  in the warp and weft directions from these stress-strain curves. In the uniaxial tension tests, relative yarn rotations do not occur and thus the yarn spacing remains unchanged. However, when the fabric undergoes shear deformations, yarn rotations induce a change in the tangent longitudinal moduli. In order to capture this effect, the approximate bilinear functions for the tangent longitudinal moduli are factored by a nondimensional yarn spacing parameter which is defined as follows. Figure 10 shows the configuration of the yarns in the initial and deformed configurations. The yarn spacing parameters  $L_\alpha$  and  $L_\beta$  for the warp and weft directions respectively are defined as the ratio between the yarn spacing in the deformed

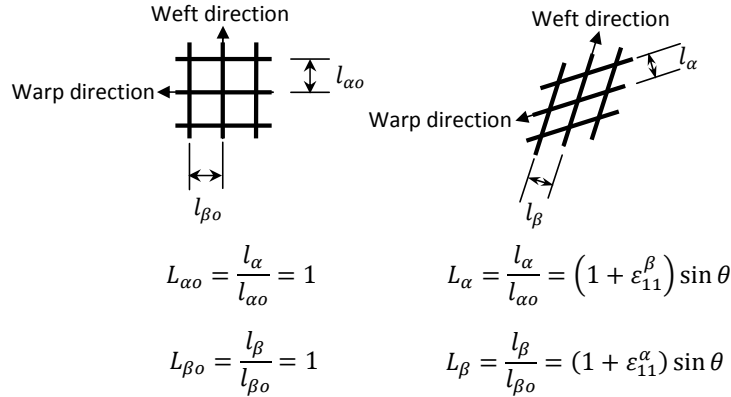


**Figure 10.** Yarn spacing parameters: initial and deformed configurations.

configuration ( $l_\alpha$  and  $l_\beta$ ) to the initial yarn spacing ( $l_{\alpha 0}$  and  $l_{\beta 0}$ ).

$$L_\alpha = \frac{l_\alpha}{l_{\alpha 0}}, \quad L_\beta = \frac{l_\beta}{l_{\beta 0}}. \quad (8)$$

The nondimensional yarn spacing parameters are equal to 1 in the initial configuration. In the deformed configuration they are obtained from the geometry as a function of the yarn direction strains  $\varepsilon_{11}^\alpha$  and  $\varepsilon_{11}^\beta$  and the angle between the yarns ( $\theta = \alpha - \beta$ ) as

$$L_\alpha = \frac{l_\alpha}{l_{\alpha 0}} = (1 + \varepsilon_{11}^\beta) \sin \theta, \quad L_\beta = \frac{l_\beta}{l_{\beta 0}} = (1 + \varepsilon_{11}^\alpha) \sin \theta. \quad (9)$$

Initially, as the yarn direction strains are zero and the angle between the yarns is  $\pi/2$ , the values of  $L_\alpha$  and  $L_\beta$  become 1, which is consistent with the definition of the yarn spacing parameters. Using the yarn spacing parameters, the tangent longitudinal moduli at each increment are approximated by

$$E_1^\alpha = \frac{1}{L_\alpha} \begin{cases} E_1^{\alpha 1} & \text{for } \varepsilon_{11}^\alpha \leq \varepsilon_{11}^{\alpha 0}, \\ E_1^{\alpha 2} & \text{for } \varepsilon_{11}^\alpha > \varepsilon_{11}^{\alpha 0}, \end{cases} \quad E_1^\beta = \frac{1}{L_\beta} \begin{cases} E_1^{\beta 1} & \text{for } \varepsilon_{11}^\beta \leq \varepsilon_{11}^{\beta 0}, \\ E_1^{\beta 2} & \text{for } \varepsilon_{11}^\beta > \varepsilon_{11}^{\beta 0}, \end{cases} \quad (10)$$

where the superscript '0' indicates the bilinear transition strain. For neat K706 style fabric, the values of the various constant material parameters in (10) are obtained from linear curve fits to the uncrimping and elongation regimes of the warp and weft direction stress-strain curves as

$$\begin{aligned} E_1^{\alpha 1} &= 1.5 \text{ GPa}, & E_1^{\alpha 2} &= 22.0 \text{ GPa}, & \varepsilon_{11}^{\alpha 0} &= 0.025, \\ E_1^{\beta 1} &= 1.8 \text{ GPa}, & E_1^{\beta 2} &= 23.0 \text{ GPa}, & \varepsilon_{11}^{\beta 0} &= 0.016. \end{aligned} \quad (11)$$

When the yarns undergo rotations due to shear deformations, the yarn spacing reduces. This causes the yarn spacing parameter to decrease. Thus, the tangent longitudinal moduli which are inversely proportional to the yarn spacing parameters increase as the yarn spacing reduces. This reflects the phenomenon of increase in yarn direction moduli due to increase in friction between adjacent yarns as they become closely packed.

The transverse moduli and the shear modulus are estimated from the 45° off-axis tension tests. The mechanism by which the fabric resists shear loads transitions from one predominantly due to rotation of yarns to one due to the transverse compression of adjacent yarns as the relative angle between the yarns approaches the locking angle. Hence, the shear rigidity is very low during the initial phase of the deformation. Once the locking angle is reached, the yarns become closely packed and further deformation is resisted by compression of yarns in the transverse direction and the occurrence of out-of-plane wrinkling. We introduce this effect into the constitutive relations by assuming that the shear modulus (which is attributed to the initial yarn rotations) to be constant and that the highly nonlinear behavior at higher displacements are caused by variation in the transverse moduli. The load-displacement curves for the 45° off-axis tension test can be converted to an equivalent shear stress-shear angle curve using the kinematic relations for an equivalent picture frame test [Milani et al. 2010]. Comparisons show that both these curves have nearly the same slope at low values of displacement/ strain. Under these assumptions, the shear modulus is estimated from the initial slope of the load-displacement curves from off-axis tension tests. The individual shear moduli for the warp and weft layers are indistinguishable. Both  $G_{12}^\alpha$  and  $G_{12}^\beta$  are assumed to be equal and to be the same as that of a single layer of fabric. For neat K706, the shear modulus is calculated from the initial slope of the curve as

$$G_{12}^\alpha = G_{12}^\beta = G_{12} = 0.4 \text{ MPa}. \quad (12)$$

The parameters  $E_2^\alpha$  and  $E_2^\beta$  are obtained from the load-displacement curves using a nonlinear fitting function that depends on the yarn spacing parameters. When the cross yarns undergo large rotation, the parallel yarns are packed together. The stresses in transverse direction prevent the parallel yarns from being too close to each other under large shear deformation. The tangent transverse moduli  $E_2^\alpha$  and  $E_2^\beta$  could be calculate from these transverse stresses. Since both  $E_2^\alpha$  and  $E_2^\beta$  attribute to prevent the further yarn rotation, we assume they are the same nonlinear function in terms of nondimensional yarn spacing  $L_\alpha$  and  $L_\beta$ . The form of the fitting function is such that as the yarn spacing parameters tend towards a limiting value ( $L_{\text{lock}}$ ), after which further yarn rotations cannot occur, the transverse moduli increase rapidly. The function and the constants  $E_2^0$  and  $L_{\text{lock}}$  are found by means of a trial and error procedure using numerical simulations as

$$E_2^\alpha = \frac{E_2^0}{L_\alpha - L_{\text{lock}}}, \quad E_2^\beta = \frac{E_2^0}{L_\beta - L_{\text{lock}}} \quad E_2^0 = 2.3 \text{ MPa}, \quad \text{with } L_{\text{lock}} = 0.68. \quad (13)$$

Table 3 summarizes the material parameters estimated for five styles of neat and 24 wt% nanoparticle impregnated Kevlar fabrics. The mechanical properties of the five styles of fabrics are quite different. The material parameter  $G_{12}$  reflects the initial shear stiffness in the off-axis tension. Parameter  $E_2^0$  provides the transverse stiffness which prevents the parallel yarns from being too close to each other. Both  $G_{12}$  and  $E_2^0$  are directly related to the final shear rigidity under large deformation. Nanoparticles largely enhance the shear rigidity. Fabrics with nanoparticles have much larger values of both  $G_{12}$  and  $E_2^0$ .

## 5. Comparison of experimental and numerical results

The constitutive model was implemented as a user-defined material subroutine (UMAT) in ABAQUS/Standard. The rectangular fabric specimen was modeled using four-node plane stress shell elements.

Style	nanopart. (wt%)	$E_1^{\alpha 1}$ (GPa)	$E_1^{\alpha 2}$ (GPa)	$\varepsilon_{11}^{\alpha 0}$	$E_1^{\beta 1}$ (GPa)	$E_1^{\beta 2}$ (GPa)	$\varepsilon_{11}^{\beta 0}$	$G_{12}$ (MPa)	$E_2^0$ (MPa)	$L_{lock}$
K310	0	0.7	20.0	0.028	6.0	23.5	0.003	0.01	0.5	0.70
	24	1.8	20.0	0.030	6.0	23.5	0.003	0.6	3.2	0.75
K706	0	1.5	22.0	0.025	1.8	22.0	0.016	0.4	2.3	0.68
	24	3.0	22.0	0.027	3.0	22.0	0.017	1.5	7.5	0.73
K720	0	1.0	22.5	0.018	1.0	26.0	0.014	0.15	0.45	0.60
	24	3.0	22.5	0.020	2.5	26.0	0.015	1.5	5.0	0.75
K745	0	0.3	16.0	0.034	0.5	18.0	0.019	0.07	0.5	0.67
	24	2.0	16.0	0.037	1.5	18.0	0.020	1.7	11.0	0.77
K779	0	0.7	17.0	0.093	7.0	22.5	0.005	0.15	3.0	0.88
	24	1.7	17.0	0.099	14.0	22.5	0.010	9.0	9.5	0.93

**Table 3.** Material parameters for five styles of neat and 24 wt% nanoparticle impregnated Kevlar fabrics.

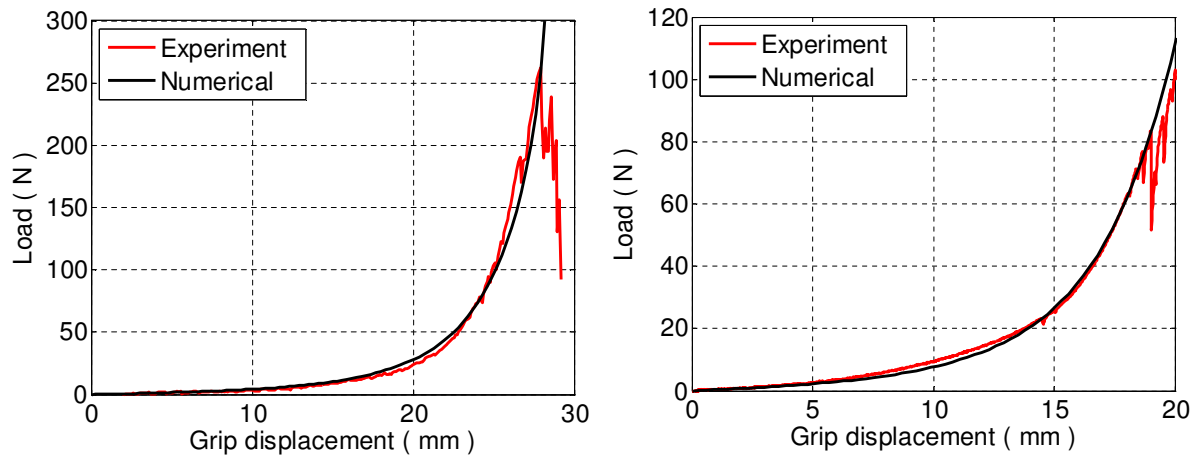


**Figure 11.** Experimental and numerical load-displacement curves for a 45° (left) and a 30° (right) off-axis tension test using neat K706 style fabric.

One edge was fixed and a prescribed displacement was applied to the opposite edge. Validation of the constitutive model is carried out by comparing the experimental result and the numerical simulation of the 30° off-axis tension test. Figure 11 shows the experimental load-displacement curves and the result of numerical simulations for 45° and 30° off-axis tension tests using neat K706. Numerical simulations fit the experimental data very well until the onset of failure. Figure 12 shows the snapshot of deformed specimen at grip displacement of 18 mm. Only the upper half of the specimen is shown. The middle line which was horizontal before loading tilts gradually when grip moves. The simulated tilting angle is almost the same as the experimental one. Overall, the simulated specimen shape agrees well with the image taken from the experiments.

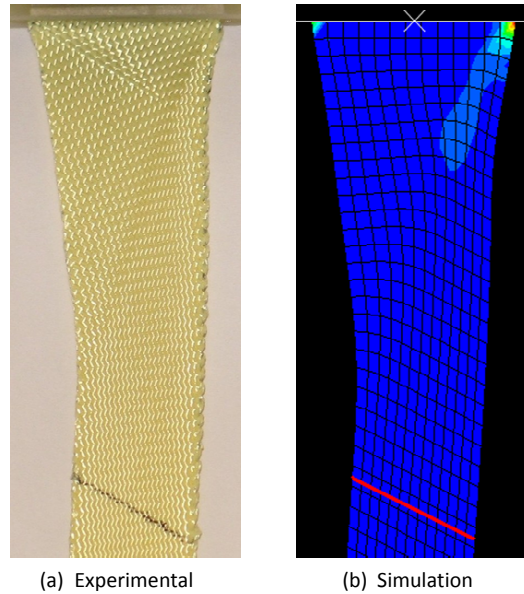


**Figure 12.** A snapshot of the deformation in a  $30^\circ$  off-axis tension test using neat K706 style fabric at a grip displacement of 18 mm.

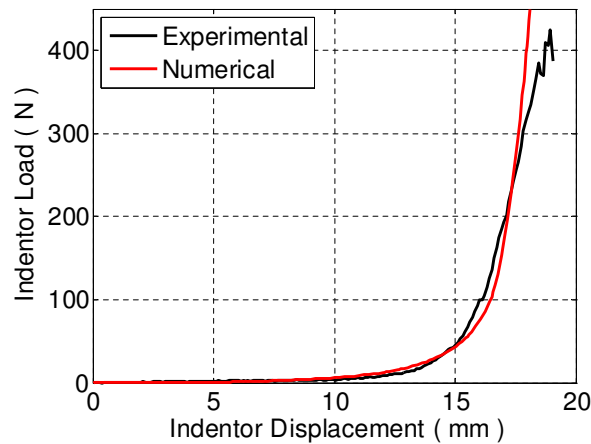


**Figure 13.** Experimental and numerical load displacement curves from a static indentation test on  $45^\circ$  neat K706 style fabric.

In the numerical simulation for the static indentation test, the fabric was meshed using four-node shell elements, the indenter was modeled as a rigid body and a frictionless contact definition was given between the indenter and the fabric. The indenter load was measured from the out-of-plane reaction force. Comparison of the experimental and numerical indenter load-displacement curves is presented in Figure 13. The numerical simulations fit the experimental data very well until failure of the fabric begins due to the slipping of yarns at the corners. Since this model does not account for damage, the simulation starts to deviate from the experimental results at large loads.

## 6. Conclusions

In-plane mechanical properties of five styles of Kevlar fabrics were investigated to show the difference between the neat fabric and the silica nanoparticle impregnated fabrics. The nanoparticles impart substantial increase to the in-plane shear rigidity. When off-axis load is applied, nanoparticle impregnated fabrics sustained higher failure loads. SEM images reveal that the nanoparticles are lodged in the interyarn and interfiber spaces in the fabric. This increases the friction between adjacent and cross yarns thereby augmenting the fabric's resistance to applied loads.

A two dimensional homogenized continuum constitutive model was developed to characterize the nonlinear anisotropic material properties of the neat and nanoparticle impregnated fabrics under large shear deformation. The material parameters required in this model were obtained from uniaxial tension and 45° off-axis tension tests. The constitutive model was interfaced with the commercial finite element code ABAQUS via a user-defined material subroutine (UMAT). Validation of the model was done by simulating a 30° off-axis tension test and a static indentation test. The simulated load-displacement curves were found to agree very well with the experimental data. This model can be used to predict the load deflection behavior of neat and nanoparticle impregnated plain woven Kevlar fabrics with good accuracy.

## Acknowledgement

This work was supported by an ARO grant W911NF-05-2-0006. Dr. David Stepp was the program manager. We also wish to thank Dr. Eric Wetzel, who provided the Kevlar fabrics used in this study.

## References

- [Decker et al. 2007] M. J. Decker, C. J. Halbach, C. H. Nam, N. J. Wagner, and E. D. Wetzel, "Stab resistance of shear thickening fluid (STF)-treated fabrics", *Compos. Sci. Tech.* **67** (2007), 565–578.
- [Grujicic et al. 2009] M. Grujicic, W. C. Bell, G. Arakere, T. He, and B. A. Cheeseman, "A meso-scale unit-cell based material model for the single-ply flexible-fabric armor", *Mater. Design* **30**:9 (2009), 3690–3704.
- [Harrison et al. 2004] P. Harrison, M. J. Clifford, and A. C. Long, "Shear characterisation of viscous woven textile composites: a comparison between picture frame and bias extension experiments", *Compos. Sci. Technol.* **64**:10-11 (2004), 1453–1465.
- [Kalman et al. 2009] D. P. Kalman, R. L. Merrill, N. J. Wagner, and E. D. Wetzel, "Effect of particle hardness on the penetration behavior of fabrics intercalated with dry particles and concentrated particle-fluid suspensions", *ACS Appl. Mat. Interf.* **1**:11 (2009), 2602–2612.
- [King et al. 2005] M. J. King, P. Jearanaisilawong, and S. Socrate, "A continuum constitutive model for the mechanical behavior of woven fabrics", *Int. J. Solids Struct.* **42**:13 (2005), 3867–3896.
- [Lebrun et al. 2003] G. Lebrun, M. N. Bureau, and J. Denault, "Evaluation of bias-extension and picture-frame test methods for the measurement of intraply shear properties of PP/glass commingled fabrics", *Compos. Struct.* **61**:4 (2003), 341–352.
- [Lee et al. 2003] Y. S. Lee, E. D. Wetzel, and N. Wagner, "The ballistic impact characteristics of Kevlar woven fabrics impregnated with a colloidal shear thickening fluid", *J. Mater. Sci.* **38**:13 (2003), 2825–2833.
- [Lin et al. 2009] H. Lin, M. J. Clifford, A. C. Long, and M. Sherburn, "Finite element modelling of fabric shear", *Model. Simul. Mater. Sci. Eng.* **17**:1 (2009), art. #15008.
- [Lomov et al. 2006] S. V. Lomov, A. Willems, I. Verpoest, Y. Zhu, M. Barbarski, and T. Stoilova, "Picture frame test of woven composite reinforcements with a full-field strain registration", *Textile Res. J.* **76**:3 (2006), 243–252.
- [Milani et al. 2010] A. S. Milani, J. A. Nemes, G. Lebrun, and M. N. Bureau, "A comparative analysis of a modified picture frame test for characterization of woven fabrics", *Polym. Compos.* **31**:4 (2010), 561–568.

- [Mohammed et al. 2000] U. Mohammed, C. Lekakou, L. Dong, and M. G. Bader, “Shear deformation and micromechanics of woven fabrics”, *Compos. A Appl. Sci. Manuf.* **31**:4 (2000), 299–308.
- [Peng et al. 2004] X. Q. Peng, J. Cao, J. Chen, P. Xue, D. S. Lussier, and L. Liu, “Experimental and numerical analysis on normalization of picture frame tests for composite materials”, *Compos. Sci. Technol.* **64**:1 (2004), 11–21.
- [Raftenberg and Mulkern 2002] M. N. Raftenberg and T. J. Mulkern, “Quasi-static uniaxial tension characteristics of plain-woven Kevlar KM2 fabric”, technical report ARL-TR-2891, Army Research Laboratory, Aberdeen Proving Ground, MD, 2002, available at <http://tinyurl.com/RaftenbergTR2891>.
- [Tan et al. 2005] V. B. C. Tan, T. E. Tay, and W. K. Teo, “Strengthening fabric armour with silica colloidal suspensions”, *Int. J. Solids Struct.* **42**:5–6 (2005), 1561–1576.

Received 19 Feb 2009. Revised 13 Jan 2010. Accepted 28 Jan 2010.

ZHAOXU DONG: [dong-zhaoxu@cat.com](mailto:dong-zhaoxu@cat.com)

*Caterpillar Inc., 100 North East Adams Street, Peoria, IL 61629, United States*

JAMES M. MANIMALA: [jmanimal@purdue.edu](mailto:jmanimal@purdue.edu)

*Purdue University, School of Aeronautics and Astronautics, 701 W. Stadium Ave, West Lafayette, IN 47907, United States*

C. T. SUN: [sun@purdue.edu](mailto:sun@purdue.edu)

*Purdue University, School of Aeronautics and Astronautics, 701 W. Stadium Ave, West Lafayette, IN 47907, United States*

# JOURNAL OF MECHANICS OF MATERIALS AND STRUCTURES

<http://www.jomms.org>

Founded by Charles R. Steele and Marie-Louise Steele

## EDITORS

CHARLES R. STEELE Stanford University, U.S.A.  
DAVIDE BIGONI University of Trento, Italy  
IWONA JASIUK University of Illinois at Urbana-Champaign, U.S.A.  
YASUhide SHINDO Tohoku University, Japan

## EDITORIAL BOARD

H. D. BUI École Polytechnique, France  
J. P. CARTER University of Sydney, Australia  
R. M. CHRISTENSEN Stanford University, U.S.A.  
G. M. L. GLADWELL University of Waterloo, Canada  
D. H. HODGES Georgia Institute of Technology, U.S.A.  
J. HUTCHINSON Harvard University, U.S.A.  
C. HWU National Cheng Kung University, R.O. China  
B. L. KARIHALOO University of Wales, U.K.  
Y. Y. KIM Seoul National University, Republic of Korea  
Z. MROZ Academy of Science, Poland  
D. PAMPLONA Universidade Católica do Rio de Janeiro, Brazil  
M. B. RUBIN Technion, Haifa, Israel  
A. N. SHUPIKOV Ukrainian Academy of Sciences, Ukraine  
T. TARNAI University Budapest, Hungary  
F. Y. M. WAN University of California, Irvine, U.S.A.  
P. WRIGGERS Universität Hannover, Germany  
W. YANG Tsinghua University, P.R. China  
F. ZIEGLER Technische Universität Wien, Austria

## PRODUCTION

PAULO NEY DE SOUZA Production Manager  
SHEILA NEWBERY Senior Production Editor  
SILVIO LEVY Scientific Editor

Cover design: Alex Scorpan

Cover photo: Mando Gomez, [www.mandolux.com](http://www.mandolux.com)

See inside back cover or <http://www.jomms.org> for submission guidelines.

JoMMS (ISSN 1559-3959) is published in 10 issues a year. The subscription price for 2010 is US \$500/year for the electronic version, and \$660/year (+ \$60 shipping outside the US) for print and electronic. Subscriptions, requests for back issues, and changes of address should be sent to Mathematical Sciences Publishers, Department of Mathematics, University of California, Berkeley, CA 94720-3840.

JoMMS peer-review and production is managed by EditFLOW™ from Mathematical Sciences Publishers.

PUBLISHED BY

 mathematical sciences publishers

<http://www.mathscipub.org>

A NON-PROFIT CORPORATION

Typeset in L<sup>A</sup>T<sub>E</sub>X

©Copyright 2010. Journal of Mechanics of Materials and Structures. All rights reserved.

# Journal of Mechanics of Materials and Structures

Volume 5, No. 4

April 2010

---

- Mechanical behavior of silica nanoparticle-impregnated kevlar fabrics**  
ZHAOXU DONG, JAMES M. MANIMALA and C. T. SUN 529
- A generalized plane strain meshless local Petrov–Galerkin method for the micromechanics of thermomechanical loading of composites**  
ISA AHMADI and MOHAMAD AGHDAM 549
- Effective medium theories for wave propagation in two-dimensional random inhomogeneous media** JIN-YEON KIM 567
- A numerical model for masonry-like structures**  
MAURIZIO ANGELILLO, LUCA CARDAMONE and ANTONIO FORTUNATO 583
- A coupled honeycomb composite sandwich bridge-vehicle interaction model**  
MIJIA YANG and A. T. PAPAGIANNAKIS 617
- Spectral element approach to wave propagation in uncertain beam structures**  
V. AJITH and S. GOPALAKRISHNAN 637
- Energy-minimizing openings around a fixed hole in an elastic plate**  
SHMUEL VIGDERGAUZ 661
- Influence of different integral kernels on the solutions of boundary integral equations in plane elasticity** Y. Z. CHEN, X. Y. LIN and Z. X. WANG 679



1559-3959(2010)5:4;1-E